



1 Non-diffusive pitch-angle scattering of a distribution of
2 energetic particles by coherent whistler waves

3 Young Dae Yoon, Paul M. Bellan

4 ¹California Institute of Technology, Pasadena, CA 91125

5 **Key Points:**

- 6 • A much improved condition is provided for how coherent whistler waves scatter
7 the pitch-angle of energetic particles.
8 • A significant fraction of energetic, thermally distributed particles undergo this scat-
9 tering.
10 • The theory reveals a critical mechanism not contained in the widely-used second-
11 order trapping theory.

Corresponding author: Young Dae Yoon, yyoon@caltech.edu

This article has been accepted for publication and undergone full peer review but has not been through the copyediting, typesetting, pagination and proofreading process which may lead to differences between this version and the Version of Record. Please cite this article as doi: 10.1029/2020JG003111

Abstract

Whether or not coherent magnetospheric whistler waves play important roles in the pitch-angle scattering of energetic particles is a crucial question in magnetospheric physics. The interaction of a thermal distribution of energetic particles with coherent whistler waves is thus investigated. The distribution is prescribed by the Maxwell-Jüttner distribution, which is a relativistic generalization of the Maxwell-Boltzmann distribution. Coherent whistler waves are modeled by circularly polarized waves propagating parallel to the background magnetic field. It is shown that for parameters relevant to magnetospheric chorus, a significant fraction (1-5%) of the energetic particle population undergoes drastic, non-diffusive pitch-angle scattering by coherent chorus. The scaling of this fraction with the wave amplitude may also explain the association of relativistic microbursts to large-amplitude chorus. A much improved condition for large pitch-angle scattering is presented that is related to, but may or may not include the exact resonance condition depending on the particle's initial conditions. The theory reveals a critical mechanism not contained in the widely-used second-order trapping theory.

Plain Language Summary

A certain class of plasma waves called whistler waves is abundant in the Earth's magnetosphere. The interaction between whistler waves and energetic particles trapped in the Earth's magnetic field can cause the particles to escape the trap and cause pulsating auroras or damage spacecraft. Although previous studies have mostly focused on diffusive mechanisms, we show that a significant fraction of the energetic particles interacts non-diffusively or coherently with the wave. We also show that a widely-used condition for such interaction is incomplete and provide a more accurate alternative.

1 Introduction

Whistler waves are right-handed circularly polarized electromagnetic plasma waves that are ubiquitous in the Earth's magnetosphere (Gurnett & O'Brien, 1964; Burtis & Helliwell, 1969; Russell et al., 1969; Tsurutani & Smith, 1974), Jupiter's magnetosphere (Sentman & Goertz, 1978; Leubner, 1982; Tsurutani et al., 1993), and Saturn's magnetosphere (Barbosa & Kurth, 1993; Akalin et al., 2006; Hospodarsky et al., 2008). These waves are also important in the solar wind (Coroniti et al., 1982; Vocks et al., 2005), fast magnetic reconnection (Mandt et al., 1994; Bellan, 2014; Chai et al., 2016; Yoon & Bellan, 2017, 2018; Haw et al., 2019), and helicon plasma sources (Boswell, 1984; Chen & Boswell, 1997). In particular, the interaction between energetic charged particles and magnetospheric whistler waves is important since the interaction can change the pitch-angle of the particles, potentially scattering them into the loss cone of a magnetic mirror configuration such as the Earth's dipole magnetic field. Because the escaped energetic particles can cause pulsating auroras at the Earth's poles and energetic particles in general can damage spacecraft, this interaction has been the focus of many studies for decades (Kennel & Petschek, 1966; Lyons et al., 1971; Helliwell & Crystal, 1973; Lyons, 1974; Summers et al., 1998; Horne & Thorne, 2003; Albert, 2005; Omura & Summers, 2006; Tsurutani et al., 2013; A. V. Artemyev et al., 2013; A. Artemyev et al., 2016).

Relativistic wave-particle resonance has been known to be an important element of particle energization and pitch-angle scattering. Resonant interaction arises when

$$\omega - kv_z = \frac{\Omega}{\gamma}. \quad (1)$$

Here, ω is the wave frequency, k is the wavenumber parallel to the background magnetic field B_0 which is oriented in the z direction, v_z is the parallel particle velocity, and $\Omega = qB_0/m$ is the cyclotron frequency of the particle with charge q and mass m . Also, $\gamma = (1 - v^2/c^2)^{-1/2}$ is the particle Lorentz factor where v is the particle speed and c is the

59 speed of light. Kennel and Petschek (1966) first quantified the scattering mechanism by
60 which incoherent whistler waves lead to velocity space diffusion, and numerous studies
61 have further developed this mechanism (Lyons et al., 1971; Lyons, 1974; Albert, 2005;
62 Tsurutani et al., 2009). However, recent spacecraft measurements indicate that the ob-
63 served chorus bursts are, in fact, extremely coherent and that these waves, especially large-
64 amplitude ones ($\delta B/B_0 \sim 0.01$ where δB is the wave magnetic field), are directly linked
65 to electron energization, loss, and microbursts (Anderson & Milton, 1964; Cattell et al.,
66 2008; Tsurutani et al., 2009, 2013; Gao et al., 2014; Breneman et al., 2017). This link-
67 age suggests that a non-diffusive process could be governing what is observed.

68 There has thus been a continuing and substantial theoretical effort to investigate
69 the dynamics of energetic particles under coherent whistler waves. Bortnik et al. (2008)
70 numerically investigated *ad hoc* the coherent interaction between large-amplitude whistler
71 waves and relativistic particles. Lakhina et al. (2010) showed via calculations of pitch-
72 angle diffusion coefficients that coherent chorus subelements can cause rapid pitch an-
73 gle scattering, although Lakhina et al. (2010) used diffusion coefficients calculated from
74 incoherent whistler waves (Kennel & Petschek, 1966) and used non-relativistic equations
75 of motion whereas the actual wave-particle interaction involves relativistic particles (10
76 keV to MeV (Tsurutani et al., 2013; Breneman et al., 2017)). Bellan (2013) presented
77 an exact analytical calculation involving a relativistic particle in a right-handed circularly
78 polarized electromagnetic wave. This calculation showed that a certain class of particles
79 undergo quick, drastic pitch-angle scattering depending on whether the individual
80 particle's initial conditions meet a certain criterion, which will be discussed in the
81 next section. Also note that other studies have investigated this single-particle problem
82 via various methods (Roberts & Buchsbaum, 1964; Ginet & Heinemann, 1990; Qian, 2000;
83 Bourdier & Gond, 2000). However, an analysis of the importance of this mechanism for
84 a distribution of particles has not yet been done. To demonstrate importance, one must
85 show that a significant fraction of the particles in the distribution experiences this drastic
86 scattering. If this can be demonstrated, then the particle interaction with coherent
87 whistler waves will be a dominant pitch-angle scattering mechanism.

88 We extend in this paper the analysis presented in Bellan (2013) to the relativistic
89 generalization of a thermal distribution of particles; the generalization is prescribed
90 by the Maxwell-Jüttner distribution (Jüttner, 1911). It is found that for parameters relevant
91 to magnetospheric chorus, coherent right-handed circularly polarized waves propagating
92 parallel to the background magnetic field trigger large, non-diffusive pitch-angle
93 scatterings for a significant fraction (1% – 5%) of the energetic particles. The scaling
94 of this fraction with the wave amplitude may also explain the association of relativistic
95 microbursts to large-amplitude chorus (Breneman et al., 2017). A new condition for
96 large pitch-angle scattering is also presented; this condition specifies a certain range related
97 to Eq. 1, but may or may not include exact resonance depending on the particle
98 initial conditions. Test-particle simulations corroborate the predictions made by this analysis.
99 It is also demonstrated that the widely-used second-order trapping theory (Sudan
100 & Ott, 1971; Nunn, 1974; Omura et al., 1991, 2007, 2008) is a simplified approximation
101 of the theory presented in this paper and that this simplified approximation effectively
102 misses critical details of the wave-particle interaction. The present study illustrates that
103 coherent whistler waves are an important cause of non-diffusive pitch-angle scattering
104 and provides an accurate condition for this scattering.

105 2 Two-Valley Motion Review

106 Let us begin with a brief review of the large pitch-angle scattering mechanism presented
107 in Bellan (2013). A thorough comprehension of this single-particle mechanism is
108 essential for understanding the ensuing analysis presented here. It is assumed that the
109 wave is right-handed circularly polarized and travels parallel to a uniform background

110 magnetic field, so the total magnetic field can be expressed as $\mathbf{B} = B_0 \hat{z} + \tilde{\mathbf{B}}$ where

$$\tilde{\mathbf{B}} = \kappa B_0 [\hat{x} \sin(kz - \omega t) + \hat{y} \cos(kz - \omega t)]. \quad (2)$$

111 Here κ is the wave amplitude relative to the background B_0 . Faraday's law determines
112 the wave electric field to be:

$$\tilde{\mathbf{E}} = -\frac{\omega}{k} \hat{z} \times \tilde{\mathbf{B}} = \frac{\omega}{k} \tilde{B} [\hat{x} \cos(kz - \omega t) - \hat{y} \sin(kz - \omega t)]. \quad (3)$$

113 The relativistic Lorentz force equation determines the motion of a charged particle:

$$\frac{d}{dt}(\gamma \boldsymbol{\beta}) = \frac{q}{m} \left(\frac{\tilde{\mathbf{E}}}{c} + \boldsymbol{\beta} \times \mathbf{B} \right) \quad (4)$$

114 where $\boldsymbol{\beta} = \mathbf{v}/c$ and $\gamma = (1 - \beta^2)^{-1/2}$.

115 In Bellan (2013), a left-handed circularly polarized wave was used although the study
116 was intended for right-handed waves. However, the result therein is unaffected by this
117 apparent error because the sign of the particle charge was unspecified. Although it was
118 not explicitly stated, the analysis was carried out assuming that the charge is positive,
119 e.g., for positrons or ions. If the charge is assumed to be negative, the same wave-particle
120 interaction arises when the wave is assumed to have a right-handed polarization. There-
121 fore, the theory in Bellan (2013) describes wave-particle interactions between positively
122 charged particles and left-handed waves, and equivalently between negatively charged
123 particles and right-handed waves — or electrons and right-handed whistler waves. This
124 equivalence can also be seen using charge-parity-time symmetry, which is a fundamen-
125 tal law of any Lorentz-invariant system (Greenberg, 2002); making the changes $z \rightarrow -z$
126 and $t \rightarrow -t$ in Eqs. 2 and 3 changes the sense of rotation of the wave, and the relevant
127 physics must be equivalent when the change $q \rightarrow -q$ is made.

128 In this paper, the analysis in Bellan (2013) with the left-handed wave and positively
129 charged particles will be used for two reasons. First, the analysis can then be kept gen-
130 eral for any particle with any sign of charge. Second, the derivation of a separate the-
131 ory for negatively charged particles will merely be a matter of some sign changes and
132 is not worth the additional complexity in understanding the core points of this paper.

133 In Bellan (2013), a “frequency mismatch” parameter

$$\xi = 1 + \alpha \gamma (n \beta_z - 1) \quad (5)$$

134 was defined, where $\alpha = \omega/\Omega$ is the normalized frequency, $\beta_z = v_z/c$ is the normal-
135 ized parallel velocity, and $n = ck/\omega$ is the refractive index. Equation 1 is satisfied when
136 $\xi = 0$, so ξ is a measure of the departure from resonance. An exact rearrangement of
137 Eq. 4 leads to an equation of motion for a particle moving in ξ -space (Bellan, 2013):

$$\frac{1}{\Omega'} \frac{d^2 \xi}{dt'^2} = -\frac{\partial \psi}{\partial \xi} \quad (6)$$

138 where

$$\psi(\xi) = \frac{1}{8} \xi^4 + \left(\kappa'^2 - \frac{\xi_0^2}{2} - s \kappa' \sin \phi_0 \right) \frac{\xi^2}{2} - \kappa'^2 \xi \quad (7)$$

139 is the pseudo-potential for ξ -space motion. Here the primed quantities are calculated in
140 the wave frame, i.e., a frame moving with a velocity $\hat{z}\omega/k$. The subscript 0 refers to the
141 value at the initial time $t = t' = 0$ and there are two parameters, namely s and ϕ_0 .

142 The parameter s is defined as

$$s = \frac{\alpha n \beta_{\perp 0} \gamma_0}{\gamma_T} = \frac{k \rho_0}{\gamma_T} \quad (8)$$

143 where $\gamma_T = (1 - n^{-2})^{-1/2}$ is the Lorentz factor of the wave, and ρ is the relativistic
 144 Larmor radius. The parameter ϕ_0 is defined as the initial angular orientation of the per-
 145 pendicular velocity in the $x - y$ plane, i.e., the angle between $\beta_{\perp 0}$ and $\tilde{E}(t = 0, z =$
 146 $0)$. The shape of the pseudo-potential is entirely determined by the initial conditions of
 147 the particle with respect to the wave as prescribed by ξ_0 , s , and ϕ_0 . Note that s is an
 148 initial condition of the particle because α and n are fixed parameters in the present anal-
 149 ysis.

150 Multiplying Eq. 6 by $d\xi/dt'$ and integrating with respect to t' yields the particle
 151 pseudo-energy,

$$W = \frac{1}{2\Omega'^2} \left(\frac{d\xi}{dt'} \right)^2 + \psi(\xi), \quad (9)$$

152 which is a constant of the motion. For certain initial conditions, $\psi(\xi)$ consists of two val-
 153 leys separated by a hill in between. If the initial particle pseudo-energy is sufficiently large
 154 to go over the hill between the two valleys, then the particle undergoes two-valley mo-
 155 tion in ξ -space. This motion involves large changes in ξ and thus in β_z , β_{\perp} and the pitch-
 156 angle $\theta_{\text{pitch}} = \tan^{-1} \beta_{\perp}/\beta_z$.

157 3 Two-Valley Motion Condition

158 Let us now derive the conditions for two-valley motion for a given particle. The
 159 conditions consist of two parts: $\psi(\xi)$ must first be two-valleyed, and the particle must
 160 have sufficient pseudo-energy to overcome the hill between the two-valleys. The initial
 161 particle kinetic pseudo-energy can be expressed as (Bellan, 2013)

$$\frac{1}{2\Omega'^2} \left(\frac{d\xi}{dt'} \right)^2_{t'=t=0} = \frac{1}{2} s^2 \kappa'^2 \cos^2 \phi_0, \quad (10)$$

162 so the total pseudo-energy is

$$W = \frac{1}{2} s^2 \kappa'^2 \cos^2 \phi_0 - \frac{\xi_0^4}{8} + \frac{\xi_0^2}{2} \kappa' (\kappa' - s \sin \phi_0) - \kappa'^2 \xi_0. \quad (11)$$

163 We write Eq. 7 as $\psi(\xi) = \xi^4/8 + b\xi^2/2 - \kappa'^2 \xi$ where $b = \kappa'^2 - \xi_0^2/2 - s\kappa' \sin \phi_0$. Then
 164 $d\psi/d\xi = \xi^3/2 + b\xi - \kappa'^2$, so one extremum is at small $\xi \simeq \kappa'^2/b$ and two extrema are
 165 at large $\xi \simeq \pm\sqrt{-2b}$. Since $d^2\psi/d\xi^2 = 3\xi^2/2 + b$, for $b < 0$ the large extrema are local
 166 minima (two valleys) and the small extremum is a local maximum (a hill). For $b \geq 0$,
 167 the large extrema are undefined, so there is a minimum at $\xi \simeq \kappa'^2/b$. Figure 1a shows
 168 an example of a two-valley $\psi(\xi)$ for which $b < 0$, and Fig. 1b shows a one-valley $\psi(\xi)$
 169 for which $b \geq 0$.

170 We now make the assumption

$$\kappa' \ll s, \quad (12)$$

171 which will be shown in Section 5 to be appropriate for relevant magnetospheric situa-
 172 tions. Then, $b \simeq -\xi_0^2/2 - s\kappa' \sin \phi_0$ is negative for

$$\xi_0^2 \geq -2s\kappa' \sin \phi_0. \quad (13)$$

173 All particles having $\sin \phi_0 > 0$ satisfy this equation because ξ_0^2 is non-negative. Par-
 174 ticles having $\sin \phi_0 \leq 0$ satisfy Eq. 13 only if they are a certain distance away from ex-
 175 act resonance ($\xi = 0$).

176 Now, inserting $\xi = \kappa'^2/b$ in Eq. 7, we have the height of the hill to be $\psi_{max} \simeq$
 177 $-\kappa'^4/(2b)$. Therefore, the particle has enough pseudo-energy to cross over the hill if

$$\frac{1}{2} s^2 \kappa'^2 \cos^2 \phi_0 - \frac{\xi_0^4}{8} + \frac{\xi_0^2}{2} \kappa' (\kappa' - s \sin \phi_0) \geq \kappa'^2 \xi_0 - \frac{\kappa'^4}{2b}. \quad (14)$$

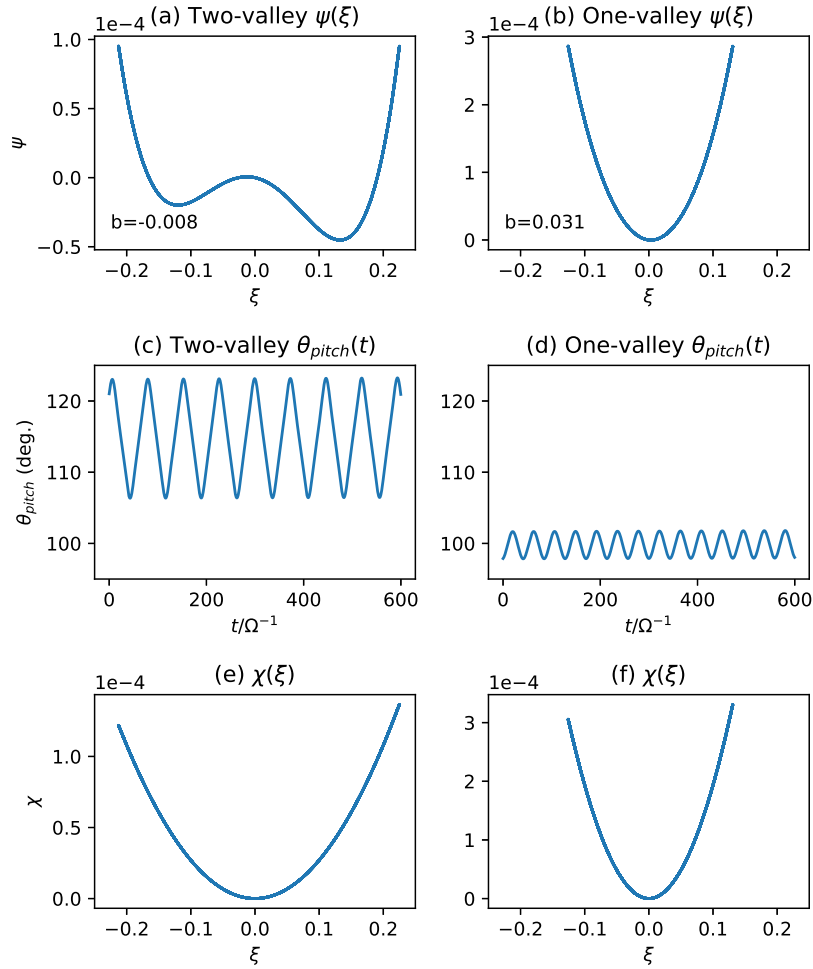


Figure 1. (a) An example of a two-valley $\psi(\xi)$ for which $b = -0.008 < 0$. (b) An example of a one-valley $\psi(\xi)$ for which $b = 0.031 \geq 0$. (c) The time-dependent pitch-angle of the particle undergoing two-valley motion, and (d) that of the particle undergoing one-valley motion. The wave parameters were $\kappa = 0.01$, $\alpha = 0.25$, and $n(\alpha) = 18$ from Eq. 28. (e), (f) The approximated pseudo-potentials χ obtained by keeping only the term involving $s\kappa'$ in Eq. 7 for the respective particles.

178 We now assume and justify later that the terms on the right-hand side of Eq. 14 are much
 179 smaller than those on the left-hand side. Using Eq. 12, Eq. 14 becomes

$$\frac{1}{2}s^2\kappa'^2 \cos^2 \phi_0 - \frac{\xi_0^4}{8} - \frac{\xi_0^2}{2}\kappa' s \sin \phi_0 \geq 0, \quad (15)$$

180 whose solution is

$$\xi_0^2 \leq 2s\kappa' (1 - \sin \phi_0). \quad (16)$$

181 Now we derive the conditions for which the assumptions regarding Eq. 14 are valid. This
 182 is done by using the solution (i.e., Eq. 16) obtained under the assumptions and deriv-
 183 ing the conditions for which the terms on the right-hand side of Eq. 14 are indeed small
 184 compared to those on the left-hand side. Using Eq. 16 as an equality, it is seen that each
 185 term on the left-hand side of Eq. 14 is $O(s^2\kappa'^2)$ except for the $\kappa'^2\xi_0^2/2$ term which is
 186 ignored by Eq. 12. On the right-hand side, $\kappa'^2\xi_0 = O(\sqrt{s\kappa'^5})$ so it can be ignored if
 187 $\kappa' \ll s^3$. Examining the second term, $\kappa'^4/2b = O(\kappa'^3/s)$ because $b = O(s\kappa')$, so it
 188 can be ignored if $\kappa' \ll s$. Since $\kappa' \ll 1$ for linear waves, $\kappa' \ll s^3$ and $\kappa' \ll s$ are both
 189 true for $s \geq 1$, and $\kappa' \ll s^3$ is a stronger statement than $\kappa' \ll s$ if $s < 1$. Therefore,
 190 for $\kappa' \ll s^3$ – which will later be demonstrated to be valid for relevant magnetospheric
 191 parameters – the following gives the condition for which a particle undergoes two-valley
 192 motion and thus a large pitch-angle scattering:

$$-2s\kappa' \sin \phi_0 \leq \xi_0^2 \leq 2s\kappa' (1 - \sin \phi_0). \quad (17)$$

193 Equation 17 is one of the main results of this paper. For $\phi_0 \geq 0$, Eq. 17 becomes Eq.
 194 16 and specifies a certain range around $\xi_0 = 0$. However, for $\phi_0 < 0$ that statistically
 195 represents half of the particle population, Eq. 17 does not include $\xi_0 = 0$, which means
 196 that particles further away from exact resonance undergo two-valley motion and thus
 197 large pitch-angle scattering. Therefore, Eq. 17 specifies the exact range of the initial dis-
 198 tance from resonance that leads to two-valley motion.

199 Figure 1c shows the time-dependent pitch-angle $\theta_{\text{pitch}}(t)$ of the particle that has
 200 enough pseudo-energy to undergo two-valley motion in the two-valley pseudo-potential
 201 in Fig. 1a. Figure 1d shows $\theta_{\text{pitch}}(t)$ of the particle moving in the one-valley pseudo-potential.
 202 The particle in Fig. 1c experiences a much larger change in pitch-angle than that in Fig.
 203 1d. The rate of change of the pitch-angle in Fig. 1c is also very large; the wave period
 204 is $T_{\text{wave}}\Omega = 2\pi/\alpha \simeq 25$, so the pitch-angle changes by $\sim 15^\circ$ in $t\Omega \simeq 40$ or in about
 205 one to two wave periods.

206 4 Distribution of ξ

207 The initial particle distribution in ξ -space will now be derived. The subscript zero
 208 will henceforth be dropped because only the initial conditions are being examined. The
 209 thermal distribution is assumed to be the Maxwell-Jüttner distribution (Jüttner, 1911)
 210 with an isotropic temperature. This is the relativistic generalization of the Maxwell-Boltzmann
 211 distribution and can be expressed in terms of the Lorentz factor γ as

$$f_\gamma = \frac{\gamma^2 \sqrt{1 - 1/\gamma^2}}{\Theta K_2(1/\Theta)} \exp\left(-\frac{\gamma}{\Theta}\right), \quad (18)$$

212 where $\Theta = k_B T/mc^2$ is the normalized temperature and K_n is the modified Bessel func-
 213 tion of the second kind of order n . This distribution is a considerable simplification, and
 214 repercussions of this simplification and possible remedies will be discussed in Section 7.
 215 Using $\gamma = \sqrt{1 + \bar{p}^2/m^2c^2} = \sqrt{1 + \bar{p}^2}$ where $\bar{\mathbf{p}} = \mathbf{p}/mc$ is the normalized particle mo-
 216 mentum, Eq. 18 can be expressed as

$$f_{\bar{\mathbf{p}}} = \frac{1}{4\pi\Theta K_2(1/\Theta)} \exp\left(-\frac{\sqrt{1 + \bar{p}^2}}{\Theta}\right). \quad (19)$$

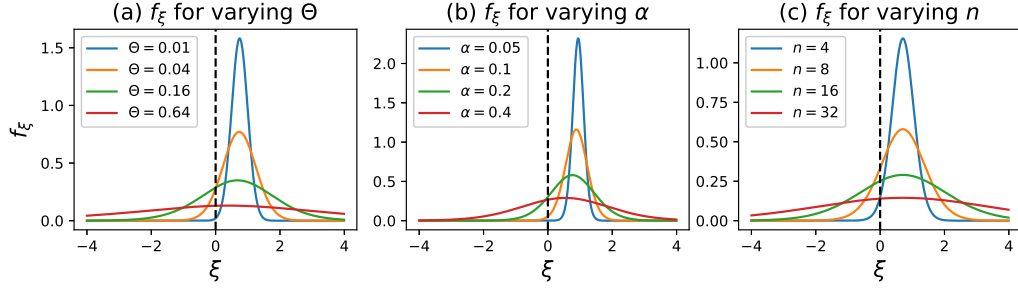


Figure 2. f_ξ for different (a) Θ , (b) α and (c) n values. The default values are $\Theta = 0.1$, $\alpha = 0.25$, and $n = 10$. The black dashed line is the resonant condition $\xi = 0$.

Integrating Eq. 19 in \bar{p}_z and over all angles gives $f_{\bar{p}_\perp}$:

$$f_{\bar{p}_\perp} = \frac{\bar{p}_\perp \sqrt{1 + \bar{p}_\perp^2}}{\Theta K_2(1/\Theta)} K_1 \left(\frac{\sqrt{1 + \bar{p}_\perp^2}}{\Theta} \right). \quad (20)$$

Note that $f_{\bar{\mathbf{p}}}$ is defined in 3D $\bar{\mathbf{p}}$ -space so that $\int f_{\bar{\mathbf{p}}} d^3 \bar{\mathbf{p}} = 1$, whereas $f_{\bar{p}_\perp}$ is defined in 1D \bar{p}_\perp -space so that $\int f_{\bar{p}_\perp} d\bar{p}_\perp = 1$. Integrating Eq. 19 in \bar{p}_x and \bar{p}_y gives $f_{\bar{p}_z}$:

$$f_{\bar{p}_z} = \frac{\Theta}{2K_2(1/\Theta)} \left(1 + \frac{\sqrt{1 + \bar{p}_z^2}}{\Theta} \right) \exp \left(-\frac{\sqrt{1 + \bar{p}_z^2}}{\Theta} \right), \quad (21)$$

where $\int f_{\bar{p}_z} d\bar{p}_z = 1$. The details of the derivations of $f_{\bar{p}_\perp}$ and $f_{\bar{p}_z}$ are given in Appendix A and Appendix B, respectively.

Now, noting that $\gamma\beta = \gamma\mathbf{v}/c = \mathbf{p}/mc = \bar{\mathbf{p}}$, the mismatch parameter (Eq. 5) can be expressed as

$$\xi = 1 + \alpha(n\bar{p}_z - \gamma). \quad (22)$$

The probability distribution of having a specific ξ is obtained by multiplying the probability distribution of having a certain γ by that of having the corresponding \bar{p}_z which yields the specified ξ , and then integrating over all γ (full derivation given in Appendix C). The solution is

$$f_\xi = \int_1^\infty \frac{\gamma^2 \sqrt{1 - 1/\gamma^2}}{2\alpha n K_2^2(1/\Theta)} \left(1 + \frac{\sqrt{1 + \bar{p}_z^2(\gamma, \xi)}}{\Theta} \right) \exp \left(-\frac{\gamma + \sqrt{1 + \bar{p}_z^2(\gamma, \xi)}}{\Theta} \right) d\gamma, \quad (23)$$

where $\bar{p}_z(\gamma, \xi) = [(\xi - 1)/\alpha + \gamma]/n$ is a rearrangement of Eq. 22 and $\int f_\xi d\xi = 1$. Given Θ , α and n , Eq. 23 is an integral solution for f_ξ .

Figure 2 shows f_ξ for different (a) Θ , (b) α and (c) n values. The default values are $\Theta = 0.1$, $\alpha = 0.25$, and $n = 10$, where $\alpha = 0.25$ and $\Theta = 0.1$ are relevant values for the dayside outer magnetosphere (Tsurutani et al., 2009), and $n = 18 \sim 10$ from the whistler dispersion relation (Eq. 28). The black dashed vertical line represents the resonant condition $\xi = 0$ (or equivalently Eq. 1). As Θ , α and n increase from zero, f_ξ broadens and more particles are resonant. After a certain threshold, however, too much broadening leads to the decrease of the local magnitude of $f_\xi(\xi = 0)$ and reduces the number of resonant particles. Increasing α significantly changes the mean value of ξ as well, raising this threshold higher.

5 Fraction of Particles Undergoing Two-Valley Motion

Before calculating the fraction of particles undergoing two-valley motion, the probability distribution of the limits of integration (Eq. 17) must first be derived. Again, the

238 subscript zero will be dropped. From Eq. 8, $s = \alpha n \beta_{\perp} \gamma / \gamma_T = \alpha \sqrt{n^2 - 1} \bar{p}_{\perp}$, so the
 239 relevant distribution is that of \bar{p}_{\perp} and $\sin \phi$. Equation 20 prescribes $f_{\bar{p}_{\perp}}$, and assuming
 240 that ϕ is isotropic, the probability distribution of $\Phi = \sin \phi$ is the Arcsine(-1,1) distri-
 241 bution,

$$f_{\Phi} = \frac{1}{\pi \sqrt{1 - \Phi^2}}, \quad (24)$$

242 for $\Phi \in (-1, 1)$.

We now have all the ingredients to calculate the fraction of particles that undergo two-valley motion in ξ -space and thus experience large pitch-angle scattering. This fraction can be found by calculating the probability that both Eqs. 13 and 16 (i.e., Eq. 17) are satisfied. In the case $\Phi > 0$ when Eq. 13 is always met, after defining a numerical factor $a = 2\alpha\kappa'\sqrt{n^2 - 1}$ so that $2s\kappa' \sin \phi = a\bar{p}_{\perp}\Phi$ and $2s\kappa' (1 - \sin \phi) = a\bar{p}_{\perp} (1 - \Phi)$, the probability of two-valley motion is

$$p_+ = \int_{\bar{p}_{\perp}=0}^{\infty} \int_{\Phi=0}^1 f_{\bar{p}_{\perp}} f_{\Phi} \int_{\xi=-\sqrt{a\bar{p}_{\perp}(1-\Phi)}}^{\sqrt{a\bar{p}_{\perp}(1-\Phi)}} f_{\xi} d\xi d\Phi d\bar{p}_{\perp}. \quad (25)$$

243 In the opposite case where $\Phi \leq 0$, the probability of two-valley motion is,

$$p_- = \int_{\bar{p}_{\perp}=0}^{\infty} \int_{\Phi=-1}^0 f_{\bar{p}_{\perp}} f_{\Phi} \left(\int_{-\sqrt{a\bar{p}_{\perp}(1-\Phi)}}^{-\sqrt{-a\bar{p}_{\perp}\Phi}} f_{\xi} d\xi + \int_{\sqrt{-a\bar{p}_{\perp}\Phi}}^{\sqrt{a\bar{p}_{\perp}(1-\Phi)}} f_{\xi} d\xi \right) d\Phi d\bar{p}_{\perp}. \quad (26)$$

244 The total fraction of particles undergoing two-valley motion is then $p_{tv} = p_+ + p_-$.

245 There are four degrees of freedom when calculating p_{tv} : Θ , α , n and κ . However,
 246 one degree of freedom can be eliminated by linking α and n through the whistler wave
 247 dispersion relation, which, for parallel propagation and $\Omega_p/\Omega \gg 1$ where Ω_p is the elec-
 248 tron plasma frequency, is

$$\frac{c^2 k^2}{\omega^2} = \frac{\Omega_p^2 / \omega^2}{|\Omega| / \omega - 1}. \quad (27)$$

249 In terms of the dimensionless variables used in this paper, this becomes

$$n = \frac{\Omega_p / \Omega}{\sqrt{\alpha(1 - \alpha)}}, \quad (28)$$

250 which can be used to express $n(\alpha)$ if Ω_p/Ω is specified. Using parameters in Tsurutani
 251 et al. (2009) ($n_e \simeq 10 \text{ cm}^{-3}$, $B_0 \simeq 125 \text{ nT}$), we obtain $\Omega_p/\Omega \simeq 8$; this value will be
 252 used throughout the rest of the analysis.

253 Let us now calculate p_{tv} for the parameters in the range $0.0001 \leq \kappa \leq 0.01$, $0.1 \leq$
 254 $\alpha \leq 0.8$ and $0.01 \leq \Theta \leq 10$ (corresponding to electron thermal energies from 5.11
 255 keV to 5.11 MeV). Since the parameter range is determined, the conditions for which
 256 the assumption $\kappa' \ll s^3$ that was used to derive Eq. 17 is true can now be determined.
 257 Because $n \gg 1$, $\kappa' = \kappa/\gamma_T = \kappa\sqrt{1 - 1/n^2} \simeq \kappa$ and $s = \alpha\sqrt{n^2 - 1}\bar{p}_{\perp} \simeq \alpha n \bar{p}_{\perp}$. From
 258 Eq. 28 it follows that $\alpha n = (\Omega_p/\Omega) \sqrt{\alpha/(1 - \alpha)}$. We now compare the largest value
 259 of κ to the lowest value of s^3 , which involves the smallest values of α and Θ . For $\Theta \ll$
 260 1, the most likely \bar{p}_{\perp} is $\sqrt{\Theta}$ (see Appendix D). Thus, the condition $\kappa' \ll s^3$ can be ex-
 261 pressed as $\kappa \ll \left((\Omega_p/\Omega) \sqrt{\alpha\Theta/(1 - \alpha)} \right)^3$, or $\Theta \gg \kappa^{2/3} / \left[(\Omega_p/\Omega)^2 (\alpha/(1 - \alpha)) \right]$. In-
 262 serting $\alpha = 0.1$ and $\kappa = 0.01$ shows that $\kappa' \ll s^3$ is valid if $\Theta \gg 0.0066$. Thus, $0.01 \leq$
 263 $\Theta \leq 10$ is consistent with $\kappa' \ll s^3$.

264 Figure 3 shows contours of p_{tv} as a function of α and Θ for different κ values. For
 265 $\kappa \geq 0.001$, which is typical for magnetospheric chorus (Tsurutani et al., 2009; Macúšová
 266 et al., 2015), a significant fraction (1%–5%) of particles undergo two-valley motion and
 267 thus large pitch-angle scattering. However, p_{tv} decreases at high Θ ($\Theta \gtrsim 1$), and this
 268 phenomenon is related to the decrease of the local magnitude of $f_{\xi}(\xi = 0)$ if there is too

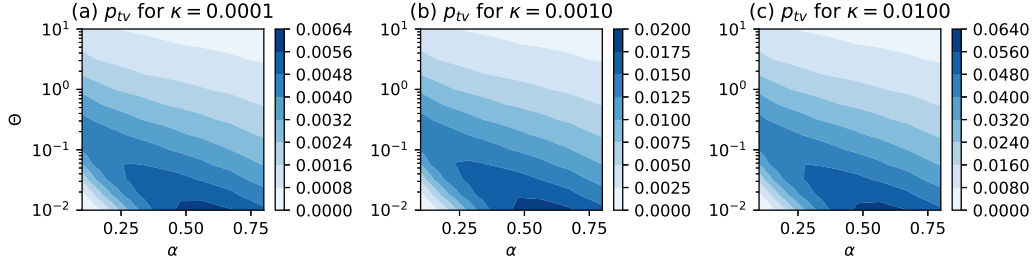


Figure 3. p_{tv} as a function of α and Θ for different κ values.

269 much broadening of f_{ξ} , as shown in Fig. 2. Figure 3 also shows that $p_{tv}(\alpha, \Theta)$ has more
 270 or less the same shape across a wide range of κ but its magnitude is proportional to $\sqrt{\kappa}$.
 271 This is because the limits of the ξ integrals in Eqs. 25 and 26 scale as $\sqrt{a} \sim \sqrt{\kappa}$, so if
 272 the integration range is sufficiently small so that the integrand may be approximated by
 273 a linear function, it follows that $p_{tv} \propto \sqrt{\kappa}$.

274 6 Numerical Verification

275 The analytical predictions presented in this paper will now be verified via numer-
 276 ical simulations. A computer code was written which solves Eq. 4 and $d\mathbf{x}/dt = c\boldsymbol{\beta}$ us-
 277 ing the fully implicit Runge-Kutta method of the Radau IIA family of order 5 (Hairer
 278 & Wanner, 1991) in the `scipy.integrate.solve_ivp` package in Python 3.7. This particular
 279 method was used because it yielded the smallest numerical error out of the available meth-
 280 ods in the Python package, measured by the drift of the average value of the pitch-angle
 281 over the full simulation time. This drift should be zero in principle because the coeffi-
 282 cients of $\psi(\xi)$ are time-independent, but numerical error introduces a small drift. For
 283 example, the simulations in Figs. 1c and 1d show that the particles' pitch-angles undergo
 284 oscillatory motion, but there are ever-so-slight, almost unnoticeable drifts ($\lesssim 0.1^\circ$) of
 285 the average values. The error was quantified by using the statistics of the 10,000 parti-
 286 cles in Fig. 5c. The Radau method with a time step $\Delta t = 0.2$ yielded a median value
 287 for the pitch-angle drift of 0.07° with a standard deviation of 0.14° , which is far smaller
 288 than the pitch-angle oscillation of a vast majority of the particles. The simulation time
 289 was set long enough for every particle to undergo at least several oscillations in the pitch-
 290 angle. The electromagnetic fields were prescribed by Eqs. 2 and 3, which is a simplified
 291 model of a whistler wave. The code was parallelized with the multiprocessing package.

292 It will first be verified that particles which satisfy Eq. 17 and thus undergo two-
 293 valley motion experience large pitch-angle scattering. 2,500 particle trajectories were nu-
 294 merically integrated, and the initial particle momenta were scanned in the range $\bar{p}_{\perp} \in$
 295 $[0, 2]$, $\bar{p}_z \in [-0.5, 0]$, and $\phi = \pi/4, -\pi/4$. The wave amplitude was $\kappa = 0.005$, and the
 296 wave frequency was $\alpha = 0.25$, which gives $n = 18$ using Eq. 28.

297 Figure 4a shows the regions of initial momentum space (dark green) that satisfy
 298 the unapproximated two-valley criteria (Eqs. 14 and $b < 0$) for $\phi = \pi/4$. Figure 4b
 299 shows regions of this space that satisfy the approximated criterion (Eq. 17). The regions
 300 are virtually identical except for $\bar{p}_{\perp} \lesssim 0.1$ because for sufficiently large \bar{p}_{\perp} , the $\kappa \ll$
 301 s^3 approximation holds. Figures 4a and 4b are effectively predictions of large pitch-angle
 302 scattering. The colors in Fig. 4c show the pitch-angle range that a particle undergoes
 303 for each point in $(\bar{p}_{\perp}, \bar{p}_z)$ space; this pitch-angle range is defined by the absolute differ-
 304 ence between the maximum and minimum pitch-angles along the particle trajectory. For
 305 example, the particle in Fig. 1c has a pitch-angle range of $\sim 15^\circ$, and that in Fig. 1d

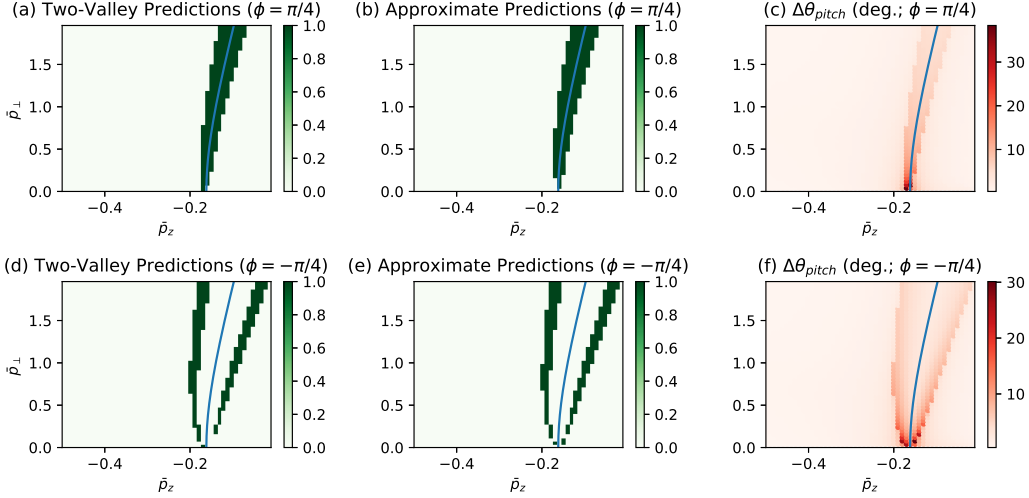


Figure 4. (a) Regions of initial momentum space (dark green) that satisfy the unapproximated two-valley criteria (Eqs. 14 and $b < 0$) for $\phi = \pi/4$. (b) Regions of this space that satisfy the approximated criterion (Eq. 17) for $\phi = \pi/4$. (c) Pitch-angle range (in degrees) within a single particle trajectory for a range of initial particle momenta for $\phi = \pi/4$. (d-f) are the same as (a-c) except for $\phi = -\pi/4$. Blue lines represent the resonance condition (Eq. 1; $\xi = 0$). The wave parameters were $\alpha = 0.25$, $\kappa = 0.005$, and $n = 18$ from Eq. 28.

306 has a pitch-angle range of $\sim 3^\circ$. Figures 4d-f are the same as Figs. 4a-c except for $\phi =$
 307 $-\pi/4$. It can be clearly seen that if a particle's initial momentum satisfies the two-valley
 308 criteria, it undergoes a large pitch-angle scattering.

309 The blue curves in Fig. 4 represent the resonance condition (Eq. 1; $\xi = 0$). The
 310 curve is found by solving $\xi = 1 + \alpha(n\bar{p}_z - \gamma) = 1 + \alpha(n\bar{p}_z - \sqrt{1 + \bar{p}_\perp^2 + \bar{p}_z^2}) = 0$ for
 311 \bar{p}_\perp (\bar{p}_z) and restricting the domain of \bar{p}_z to be consistent with $\gamma = \alpha^{-1} + n\bar{p}_z \geq 1$. In
 312 Figs. 4d-f, the blue lines do not pass through regions of two-valley motion and large scat-
 313 tering. This fact is consistent with Eq. 17 which qualitatively states that for $\phi < 0$, the
 314 condition for two-valley motion and large scattering does not include $\xi = 0$.

315 Next, the analytical prediction for p_{tv} will be verified via the Monte-Carlo method.
 316 The trajectories of 10,000 particles whose initial momenta were randomly sampled from
 317 Eq. 19 were respectively integrated for $\kappa = 0.0001, 0.001$ and 0.01 . Other parameters
 318 were $\alpha = 0.25$, $n = 18$, and $\Theta = 0.1$.

319 Figure 5 shows the pitch-angle range (in degrees) of the randomly sampled parti-
 320 cles for different κ values. Red points represent particles that meet the two-valley cri-
 321 terion (Eq. 17), and the text inside represents the percentage of red particles. Figure 3
 322 shows that for $\alpha = 0.25$ and $\Theta = 0.1$, the predicted percentage ranges are 0.4–0.48%,
 323 1.25 – 1.5% and 4.00 – 4.80% for $\kappa = 0.0001, 0.001$ and 0.01 , respectively, which ap-
 324 proximately agree with the results in Fig. 5. Red points generally experience significantly
 325 larger pitch-angle scattering than other particles, as can be seen from the median value
 326 of the red points (red horizontal lines). However, it can be seen that there are blue points
 327 that also experience large scattering; examining the pseudo-potential $\psi(\xi)$ for these points
 328 shows that these particles have pseudo-energies that are just short of overcoming the two-
 329 valley hill, so they “almost” undergo two-valley motion and experience substantial pitch-
 330 angle scattering. Therefore, we conclude that p_{tv} is a lower-bound for the fraction of par-
 331 ticles with large pitch-angle scattering.

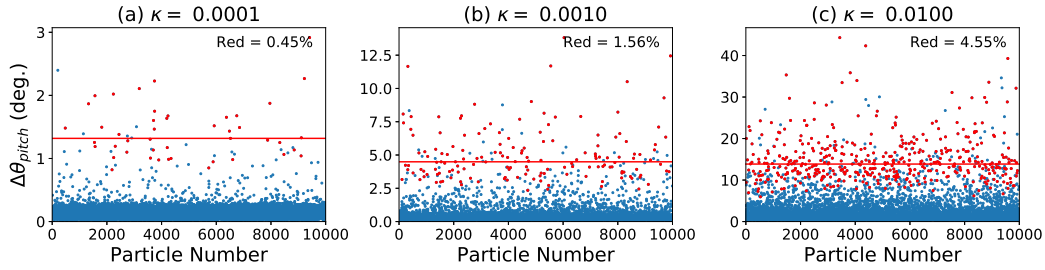


Figure 5. Pitch-angle range of 10,000 particles whose initial momenta were randomly sampled from Eq. 19 for different κ values. Red points represent particles that meet the two-valley criterion (Eq. 17), and the text inside represents the percentage of red particles. The red horizontal lines represents the median $\Delta\theta_{pitch}$ of the red particles in degrees.

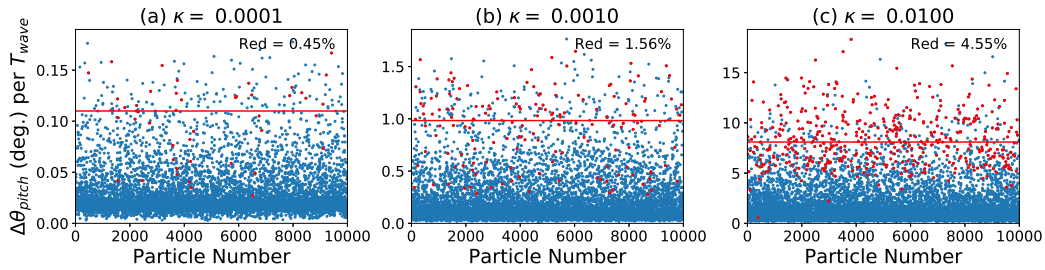


Figure 6. Pitch-angle change per wave period of the respective simulations in Fig. 5. The red horizontal lines respectively represent the median value of the pitch-angle change per wave period of the red particles.

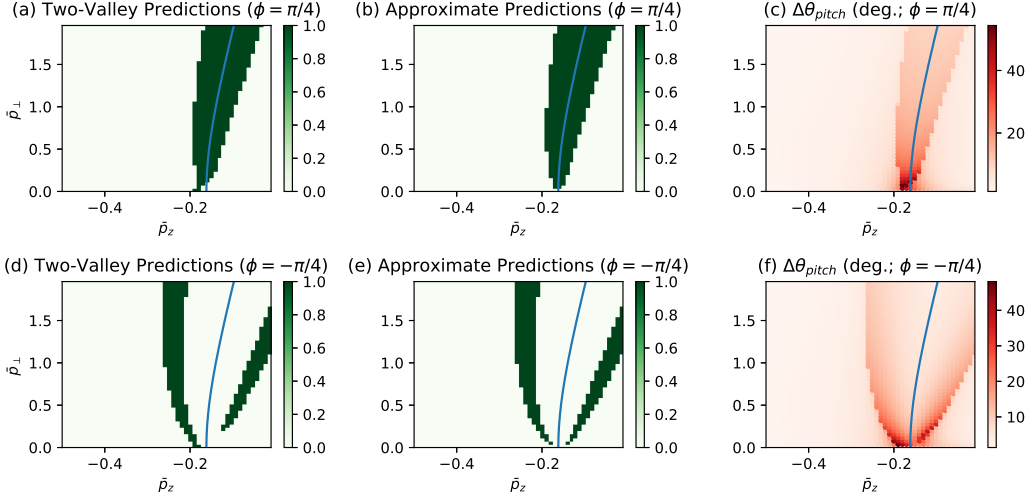


Figure 7. Same as Fig. 4, but for $\kappa = 0.02$.

332 Even if two-valley motion were to cause large pitch-angle scattering, the mechanism
 333 would not be significant if this scattering could not occur within a short enough
 334 time. Thus, it is necessary to show that the coherent wave lasts sufficiently long for two-
 335 valley motion to occur. Figure 6 shows the pitch-angle change within a single wave peri-
 336 od for the respective simulations in Fig. 5. Tsurutani et al. (2009) observed in the outer
 337 magnetosphere coherent chorus elements with amplitudes $\kappa \simeq 0.0016$ ($B_0 \simeq 125$ nT
 338 and wave field $\tilde{B} \simeq 200$ pT) that are $0.1 \sim 0.5$ s long with a frequency of ~ 700 Hz.
 339 These elements consisted of subelements or packets lasting $5 \sim 10$ ms, corresponding
 340 to about 3.5 to 7 wave periods. $\kappa \simeq 0.0016$ approximately corresponds to Fig. 6b, which
 341 shows that red particles can reach their median pitch-angle range ($\sim 5^\circ$ from Fig. 5b)
 342 in five wave periods on average. For $\kappa = 0.01$ (Fig. 6b), this rate is even faster as the
 343 red particles can reach their median pitch-angle range of $\sim 15^\circ$ (Fig. 5c) in about two
 344 wave periods.

345 7 Discussion

346 The results presented here may help explain the association of large-amplitude whistler
 347 waves to relativistic microbursts (~ 1 MeV) (Breneman et al., 2017) and may explain
 348 the lack of such energetic microbursts in small-amplitude chorus (Tsurutani et al., 2013).
 349 Particle energization is not a subject of this paper and thus will not be discussed; it will
 350 be assumed that the particles are first energized by some mechanism that yields a rel-
 351 ativistic distribution, and then the ensuing pitch-angle dynamics are studied in order to
 352 concentrate on one topic. It should be noted, however, that energization and pitch-angle
 353 scattering may occur simultaneously.

354 In Fig. 3, for small amplitudes ($0.0001 \leq \kappa \leq 0.001$), only up to 0.5% of parti-
 355 cles in a distribution with a temperature of ~ 1 MeV (corresponding to $\Theta \simeq 2$) in-
 356 teract with the wave, whereas for large amplitudes ($\kappa \simeq 0.01$), $\sim 2\%$ of such particles
 357 do. This is because the range of the two-valley condition in Eq. 17 scales with the wave
 358 amplitude κ ; i.e., as the wave amplitude increases, more particles, including energetic
 359 particles, satisfy the two-valley condition.

360 The interaction of large-amplitude waves with relativistic particles is further ex-
 361 plained in Fig. 7, which is the same as Fig. 4 but for a larger wave amplitude ($\kappa = 0.02$).

It can clearly be seen that the predictions of large scattering in Fig. 7 are much broader in phase space than those in Fig. 4. This is important because in Fig. 4, relativistic particles with $\bar{p} \gtrsim 1$ must have large initial pitch-angles to interact with the wave since the two-valley condition is a narrow range related to the exact resonance condition, and thus these particles must undergo extremely large pitch-angle scatterings in order to jump into the loss cone. However, in Fig. 7, the range for two-valley motion is much increased, allowing for relativistic particles with smaller initial pitch-angles to interact with the wave. The deviation of the two-valley condition from the exact resonance condition is because the range in Eq. 17 scales with κ . Furthermore, the pitch-angle range itself is significantly increased in Fig. 7. Therefore, a larger wave amplitude allows for relativistic particles with lower initial pitch-angles to interact with the wave, while simultaneously increasing the amount of pitch-angle scattering; these two effects lead to more relativistic particles being pitch-angle scattered into the loss-cone.

There are a few limitations to the present analysis that may be subject to future work. First, the Maxwell-Jüttner distribution is a simplification and should not be considered as a distribution representing the entire electron population. The actual distribution is a sum of these Maxwellians or other functions such as the kappa distribution (Pierrard & Lazar, 2010). If the actual distribution can be expressed as a weighted sum of Maxwell-Jüttner distributions, then the total fraction of particles that undergo two-valley motion is the sum of the partial fractions for each distribution. On the other hand, if the actual distribution is another sufficiently simple function, then an analysis similar to that in Sections 4 and 5 may be conducted by replacing Eq. 18 by the actual distribution. However, depending on the complexity of the actual distribution, its transition to Eq. 23 may be more complicated.

Second, the particle temperature is assumed for simplicity to be isotropic, whereas observations indicate that electron temperature in the magnetosphere in general is anisotropic and electron distribution functions can be more complex than simple anisotropic distributions (Li et al., 2010). The transition to an anisotropic Maxwell-Jüttner distribution is outlined in Livadiotis (2016) and Treumann and Baumjohann (2016).

Third, the wave is assumed to have exact parallel propagation, whereas many instances of magnetospheric chorus involve oblique propagation (Santolík et al., 2009; Artemyev et al., 2016). Also, chorus typically exhibits frequency and amplitude changes over a short time period (Tsurutani et al., 2009), but the model presented here is based on a plane wave with a fixed frequency and wavenumber (Eqs. 2 and 3). However, including obliquity and variable frequency makes the analysis considerably more complicated and so would be inappropriate for an inaugural analysis.

8 Comparison to Second-order Trapping Theory

A popular theory describing wave-particle interactions is the second-order trapping effect presented in, e.g., Sudan and Ott (1971), Nunn (1974) and Omura et al. (1991). Omura et al. (2007) and Omura et al. (2008) present relativistic generalizations of the theory. However, it will now be shown that this previous theory is an approximation of the theory presented here; this approximation effectively misses the critical two-valley nature of the pseudo-potential.

Omura et al. (1991) use the following coupled equations for non-relativistic speeds:

$$\frac{d\zeta}{dt} = k(v_z - V_R), \quad (29)$$

$$\frac{d}{dt}(v_z - V_R) = \frac{\omega_t^2}{k}(\sin \zeta + S), \quad (30)$$

where

$$V_R = \frac{\omega - \Omega}{k}, \quad (31)$$

ζ is the angle between \mathbf{v}_\perp and $\tilde{\mathbf{B}}$, $\omega_t = \sqrt{k v_\perp \Omega \kappa}$ is the trapping frequency, and S is a parameter that is equal to zero when the background magnetic field is spatially uniform and ω is a constant. Therefore, setting $S = 0$, differentiating Eq. 30 in time, and using Eq. 29,

$$\frac{d^2}{dt^2}(v_z - V_R) = \frac{\omega_t^2}{k} \cos \zeta \frac{d\zeta}{dt}, \quad (32)$$

$$= \omega_t^2 (v_z - V_R) \cos \zeta. \quad (33)$$

406 Letting $\gamma = 1$ in Eq. 5 and rearranging shows that

$$\xi = \frac{k}{\Omega} (v_z - V_R), \quad (34)$$

so Eq. 33 becomes

$$\frac{d^2 \xi}{dt^2} = \xi \omega_t^2 \cos \zeta, \quad (35)$$

$$= -\frac{\partial}{\partial \xi} \left(-\frac{\xi^2}{2} \omega_t^2 \cos \zeta \right), \quad (36)$$

$$\frac{1}{\Omega^2} \frac{d^2 \xi}{dt^2} = -\frac{\partial \chi(\xi)}{\partial \xi}, \quad (37)$$

407 where $\chi(\xi) = -\xi^2 \omega_t^2 \cos \zeta / 2\Omega^2$ is the pseudo-potential of this system.

Now, let us examine the term involving $s\kappa'$ in Eq. 7 assuming $\gamma_0 = \gamma_T = 1$;

$$-s\kappa \sin \phi_0 \frac{\xi^2}{2} = -\alpha n \kappa \beta_{\perp 0} \sin \phi_0 \frac{\xi^2}{2}, \quad (38)$$

$$= -\frac{\omega}{\Omega} \frac{ck}{\omega} \kappa \frac{v_{\perp 0}}{c} \sin \phi_0 \frac{\xi^2}{2}, \quad (39)$$

$$= -\frac{\omega_{t0}^2}{\Omega^2} \sin \phi_0 \frac{\xi^2}{2}, \quad (40)$$

$$= \chi_0(\xi), \quad (41)$$

408 because ζ and ϕ are related by $\zeta = \phi - \pi/2$, so $\cos \zeta = \sin \phi$. $\chi_0(\xi)$ is $\chi(\xi)$ except
 409 that $v_{\perp 0}$ and ϕ_0 are used instead of v_\perp and ϕ , and the relationship is similar for ω_{t0} and
 410 ω_t . Therefore, $\chi(\xi)$ results from keeping only the $s\kappa'$ term in $\psi(\xi)$. This is important
 411 because $\chi(\xi)$ only describes either a trapping or a non-trapping potential but not a two-
 412 valley potential.

413 Figure 1e and 1f plot the approximated pseudo-potentials $\chi(\xi)$ for the particles in
 414 Fig. 1a and 1b, respectively. For both particles, $\chi(\xi)$ is clearly a one-valley potential,
 415 whereas the unapproximated $\psi(\xi)$ is two-valleyed for the particle in Fig. 1a and thus it
 416 undergoes much larger pitch-angle scattering than the particle in Fig. 1b. Therefore,
 417 if the theory in Omura et al. (1991) were to be used, it would be impossible to distin-
 418 guish between the two particles which clearly have an extremely large difference in the
 419 amount of pitch-angle scattering.

420 Another important problem with the second-order trapping theory is that the time-
 421 dependence of the variables is ambiguous at best. Omura et al. (1991) imply that v_\perp and
 422 thus ω_t are time-dependent but then treat v_\perp as a constant when they state that com-
 423 bining Eqs. 29 and 30 gives a pendulum equation. Sudan and Ott (1971) admit that v_\perp
 424 is time-dependent, but then argue that it can be treated as a constant, as specified in
 425 the sentence after their Eq. 10. In the present theory, however, we explicitly differen-
 426 tiate between the initial variables and the time-dependent ones, so no approximation re-
 427 garding time-dependence needs to be made. This is an extremely important point be-
 428 cause this time-dependence of v_\perp gives the two-valley potential whereas treating it as
 429 a constant does not. This fact can be more explicitly illustrated by examining Eq. 26

430 in Bellan (2013) which is an equation for the parallel velocity (recall that $\beta_z = v_z/c$
431 and prime refers to the wave frame):

$$\frac{1}{\Omega'} \frac{d^2 \beta'_z}{dt'^2} = \xi \beta'_\perp \cdot \frac{\tilde{\mathbf{B}}'_\perp}{B_0} - \beta'_z \frac{\tilde{\mathbf{B}}'_\perp}{B_0} \cdot \frac{\tilde{\mathbf{B}}'_\perp}{B_0}. \quad (42)$$

432 The second-order trapping theory effectively drops the last term in Eq. 42 and ignores
433 the time-dependence of the first term on the right-hand side. This leads to

$$\frac{1}{\Omega'} \frac{d^2 \xi}{dt'^2} = \alpha n \frac{\gamma'}{\gamma_T} \xi \beta'_\perp \cdot \frac{\tilde{\mathbf{B}}'_\perp}{B_0}, \quad (43)$$

434 which is equivalent to Eq. 37 if $\gamma' = \gamma_T = 1$ is assumed. However, Eq. 35 of Bellan
435 (2013) states that

$$\beta'_\perp \cdot \frac{\tilde{\mathbf{B}}'_\perp}{B_0} = \beta'_{\perp 0} \cdot \frac{\tilde{\mathbf{B}}'_{\perp 0}}{B_0} - \frac{\gamma_T}{2\alpha n \gamma'} (\xi^2 - \xi_0^2), \quad (44)$$

436 which means that treating v_\perp as a constant effectively misses the ξ -dependence in Eq.
437 44, which is the reason for the two-valley shape of the pseudo-potential.

438 For example, neglecting the ξ_0^2 term in Eq. 44 leads to erroneous conclusions re-
439 garding the shape of the potential near $\xi = 0$. In Fig. 1e, $\chi(\xi)$ is a valley because $-s\kappa' \sin \phi_0$
440 is positive in this case. However, the correct pseudo-potential $\psi(\xi)$ in Fig. 1a is a hill
441 near $\xi = 0$ because $-\xi_0^2/2 - s\kappa' \sin \phi_0$ in Eq. 7 is negative in this case. Also, the ξ^2
442 term in Eq. 44, which leads to the positive ξ^4 term in Eq. 7, prevents the pseudo-potential
443 from diverging to $-\infty$ as $\xi \rightarrow \pm\infty$. This prevents the particle ξ from veering off to in-
444 finity; this phenomenon is unphysically allowed if the approximated $\chi(\xi)$ is used and $\sin \phi_0 >$
445 0 . The term linear in ξ in Eq. 7 which affects the asymmetry of the two-valleys is also
446 neglected in $\chi(\xi)$. The fact that v_\perp is not constant can be explicitly seen in Fig. 5g of
447 Bellan (2013), where v_\perp of a particle undergoing two-valley motion varies in time by over
448 a factor of three.

449 It should be noted, however, that for a non-uniform background field and/or time-
450 dependent wave frequencies, S is finite in Eq. 30 and this may have an important role
451 in the system additional to the effects described in the present paper. In fact, many stud-
452 ies that use the approximated second-order trapping theory focus on the non-local pro-
453 cesses where effects due to finite S are significant (e.g., in Omura et al. (2007)). The present
454 study focuses on local scattering that happens over only a few wave periods, so S can
455 be presumed to be small, and $\psi(\xi)$ instead of $\chi(\xi)$ must be used.

456 A simple way to see that S is locally negligible is to consider the physical length
457 of the wave for the duration of the pitch-angle scattering. From Figs. 5 and 6, maximum
458 deflection happens within 5 wave periods. For $B_0 = 125$ nT, $\Omega = 2.2 \times 10^4$ rad/s. Us-
459 ing wave parameters that have been used so far, $\alpha = 0.25$ gives $\omega = 5.5 \times 10^3$ rad/s,
460 and $n = 18$ gives the wavelength to be $\lambda = 19$ km. Therefore, 5 wave periods corre-
461 sponds to about 100 km, which is a minuscule distance compared to the length scale of
462 the magnetosphere at $L \simeq 5$ where plentiful amounts of relativistic microbursts occur
463 (Tsurutani et al., 2013). The time-dependence of the wave frequency is also negligible
464 because a single chorus element lasts for around 0.1-0.5 s while its frequency increases
465 by about 50%, but five wave periods corresponds to less than 0.01 s (Tsurutani et al.,
466 2009). Therefore, S can be considered to be negligible during the local scattering pro-
467 cess.

468 9 Conclusion

469 The interaction of a relativistically-consistent thermal distribution of particles with
470 a coherent right-handed circularly polarized wave has been investigated. Departure from

471 wave-particle resonance for each particle is expressed by a frequency mismatch param-
 472 eter ξ , where $\xi = 0$ represents perfect resonance. An exact rearrangement of the rel-
 473 ativistic particle equation of motion shows that ξ follows pseudo-Hamiltonian dynam-
 474 ics with an associated pseudo-potential $\psi(\xi)$. If $\psi(\xi)$ has two-valleys separated by a hill,
 475 and the particle has enough pseudo-energy to overcome the hill, then the particle under-
 476 goes two-valley ξ -space motion that produces a large, non-diffusive pitch-angle scat-
 477 tering.

478 An accurate condition for two-valley motion and thus for large pitch-angle scat-
 479 tering has been derived; this condition is related to but may or may not include the ex-
 480 act resonance condition (Eq. 1), and the range of this condition scales with the wave am-
 481 plitude. Assuming that the particle distribution is Maxwell-Jüttner, which is a relativistic
 482 generalization of the Maxwell-Boltzmann distribution, for typical magnetospheric pa-
 483 rameters a significant fraction (1 – 5%) of the particles undergoes two-valley motion.
 484 The pertinent analysis can potentially be used for the actual local electron distribution,
 485 which may not be exactly Maxwellian. Numerical simulations confirm the analytical re-
 486 sults. The scaling of the fraction of interacting particles with the wave amplitude may
 487 also explain the association of relativistic microbursts to large-amplitude chorus. The
 488 present theory is more accurate and exact than the widely-used second-order trapping
 489 theory as second-order trapping theory fails to take into account two-valley motion.

490 Appendix A Derivation of $f_{\bar{p}_\perp}$

491 In cylindrical coordinates, Eq. 19 is equivalent to

$$f_{\bar{\mathbf{p}}} d^3 \bar{\mathbf{p}} = \frac{1}{4\pi\Theta K_2(1/\Theta)} \exp\left(-\frac{\sqrt{1+\bar{p}^2}}{\Theta}\right) \bar{p}_\perp d\bar{p}_\perp d\phi d\bar{p}_z. \quad (\text{A1})$$

492 Integrating in \bar{p}_z gives

$$\int_{\bar{p}_z=-\infty}^{\infty} f_{\bar{\mathbf{p}}} \bar{p}_\perp d\bar{p}_\perp d\phi d\bar{p}_z = \int_{\bar{p}_z=-\infty}^{\infty} \frac{1}{4\pi\Theta K_2(1/\Theta)} \exp\left(-\frac{\sqrt{1+\bar{p}_\perp^2+\bar{p}_z^2}}{\Theta}\right) \bar{p}_\perp d\bar{p}_\perp d\phi d\bar{p}_z \quad (\text{A2})$$

$$= \bar{p}_\perp d\bar{p}_\perp d\phi \int_{\bar{p}_z=0}^{\infty} \frac{1}{2\pi\Theta K_2(1/\Theta)} \exp\left(-\frac{\sqrt{1+\bar{p}_\perp^2+\bar{p}_z^2}}{\Theta}\right) d\bar{p}_z, \quad (\text{A3})$$

493 where $\bar{p}^2 = \bar{p}_\perp^2 + \bar{p}_z^2$. Defining

$$a^2 = \frac{1+\bar{p}_\perp^2}{\Theta^2} \quad (\text{A4})$$

494 and

$$t = \frac{\bar{p}_z}{\Theta}, \quad (\text{A5})$$

495 the \bar{p}_z -integral in Eq. A3 becomes

$$\frac{1}{2\pi K_2(1/\Theta)} \int_0^{\infty} \exp\left(-\sqrt{a^2+t^2}\right) dt. \quad (\text{A6})$$

496 Now we define

$$t = a \sinh z, \quad (\text{A7})$$

497 so $\sqrt{a^2+t^2} = a\sqrt{1+\sinh^2 z} = a \cosh z$ and $dt = a \cosh z dz$. Equation A6 is now

$$\frac{a}{2\pi K_2(1/\Theta)} \int_0^{\infty} \cosh z \exp(-a \cosh z) dz. \quad (\text{A8})$$

498 The z -integral in Eq. A8 evaluates to $K_1(a)$ where K_n is the modified Bessel function
 499 of the second kind of order n (Zwillinger, 2015, Section 8.432, 1.).

500 Therefore, Eq. A3 is now

$$\frac{\sqrt{1+\bar{p}_\perp^2}}{2\pi\Theta K_2(1/\Theta)} K_1\left(\frac{\sqrt{1+\bar{p}_\perp^2}}{\Theta}\right) \bar{p}_\perp d\bar{p}_\perp d\phi. \quad (\text{A9})$$

501 Integrating in ϕ yields the final result:

$$f_{\bar{p}_\perp} d\bar{p}_\perp = \frac{\bar{p}_\perp \sqrt{1+\bar{p}_\perp^2}}{\Theta K_2(1/\Theta)} K_1\left(\frac{\sqrt{1+\bar{p}_\perp^2}}{\Theta}\right) d\bar{p}_\perp, \quad (\text{A10})$$

502 which is Eq. 20.

503 Appendix B Derivation of $f_{\bar{p}_z}$

504 In cylindrical coordinates, Eq. 19 is equivalent to

$$f_{\bar{\mathbf{p}}} d^3\bar{\mathbf{p}} = \frac{1}{4\pi\Theta K_2(1/\Theta)} \exp\left(-\frac{\sqrt{1+\bar{p}^2}}{\Theta}\right) \bar{p}_\perp d\bar{p}_\perp d\phi d\bar{p}_z. \quad (\text{B1})$$

505 Integrating in all ϕ and \bar{p}_\perp , Eq. B1 becomes

$$f_{\bar{p}_z} d\bar{p}_z = \int_{\bar{p}_\perp=0}^{\infty} \frac{1}{2\Theta K_2(1/\Theta)} \exp\left(-\frac{\sqrt{1+\bar{p}_\perp^2+\bar{p}_z^2}}{\Theta}\right) \bar{p}_\perp d\bar{p}_\perp d\bar{p}_z. \quad (\text{B2})$$

506 Letting $\eta^2 = 1 + \bar{p}_\perp^2 + \bar{p}_z^2$ while keeping \bar{p}_z constant so that

$$\eta d\eta = \bar{p}_\perp d\bar{p}_\perp, \quad (\text{B3})$$

507 we have

$$f_{\bar{p}_z} d\bar{p}_z = \int_{\eta=\sqrt{1+\bar{p}_z^2}}^{\infty} \frac{1}{2\Theta K_2(1/\Theta)} \exp\left(-\frac{\eta}{\Theta}\right) \eta d\eta d\bar{p}_z. \quad (\text{B4})$$

508 Using the integral formula (Zwillinger, 2015, Section 3.351, 2.)

$$\int_u^{\infty} x^n e^{-\mu x} dx = e^{-u\mu} \sum_{k=0}^n \frac{n!}{k!} \frac{u^k}{\mu^{n-k+1}}, \quad (\text{B5})$$

where $x = \eta$, $u = \sqrt{1+\bar{p}_z^2}$, $\mu = 1/\Theta$, and $n = 1$ in this case, we have

$$f_{\bar{p}_z} d\bar{p}_z = \frac{1}{2\Theta K_2(1/\Theta)} \left(\Theta^2 + \Theta\sqrt{1+\bar{p}_z^2}\right) \exp\left(-\frac{\sqrt{1+\bar{p}_z^2}}{\Theta}\right), \quad (\text{B6})$$

$$= \frac{\Theta}{2K_2(1/\Theta)} \left(1 + \frac{\sqrt{1+\bar{p}_z^2}}{\Theta}\right) \exp\left(-\frac{\sqrt{1+\bar{p}_z^2}}{\Theta}\right), \quad (\text{B7})$$

509 which is Eq. 21.

510 Appendix C Derivation of f_ξ

511 ξ is defined as

$$\xi = 1 + \alpha(n\bar{p}_z - \gamma) = 1 + \alpha\zeta, \quad (\text{C1})$$

512 where $\zeta = n\bar{p}_z - \gamma$.

f_ζ will first be derived. Defining $R = n\bar{p}_z$ (so $d\bar{p}_z = dR/n$ and $\zeta = R - \gamma$), we have

$$f_{\bar{p}_z}(\bar{p}_z)d\bar{p}_z = f_{\bar{p}_z}(R/n) \frac{dR}{n} \quad (\text{C2})$$

$$= \frac{\Theta}{2nK_2(1/\Theta)} \left(1 + \frac{\sqrt{1+R^2/n^2}}{\Theta} \right) \exp \left(-\frac{\sqrt{1+R^2/n^2}}{\Theta} \right) dR \quad (\text{C3})$$

$$= f_R(R)dR. \quad (\text{C4})$$

Now, in order for $\zeta = R - \gamma$ to be true, the value of R has to equal $\zeta + \gamma$ for a given value of γ . The probability distribution of this occurrence integrated over all values of γ gives f_ζ :

$$f_\zeta(\zeta) = \int_1^\infty f_\gamma(\gamma) f_R(\zeta + \gamma) d\gamma \quad (\text{C5})$$

$$= \int_1^\infty \frac{\gamma^2 \sqrt{1-1/\gamma^2}}{2nK_2^2(1/\Theta)} \left(1 + \frac{\sqrt{1+(\zeta+\gamma)^2/n^2}}{\Theta} \right) \exp \left(-\frac{\gamma + \sqrt{1+(\zeta+\gamma)^2/n^2}}{\Theta} \right) d\gamma. \quad (\text{C6})$$

Finally, rearranging Eq. C1 yields $\zeta(\xi) = (\xi - 1)/\alpha$ so that $d\zeta = d\xi/\alpha$. It follows that

$$f_\zeta(\zeta)d\zeta = f_\zeta([\xi - 1]/\alpha) \frac{d\xi}{\alpha} \quad (\text{C7})$$

$$= \int_1^\infty \frac{\gamma^2 \sqrt{1-1/\gamma^2}}{2\alpha n K_2^2(1/\Theta)} \left(1 + \frac{\sqrt{1+(\zeta(\xi) + \gamma)^2/n^2}}{\Theta} \right) \exp \left(-\frac{\gamma + \sqrt{1+(\zeta(\xi) + \gamma)^2/n^2}}{\Theta} \right) d\gamma d\xi \quad (\text{C8})$$

$$= f_\xi(\xi)d\xi. \quad (\text{C9})$$

Writing $\bar{p}_z(\gamma, \xi) = (\zeta(\xi) + \gamma)/n$ yields a more compact expression:

$$f_\xi(\xi) = \int_1^\infty \frac{\gamma^2 \sqrt{1-1/\gamma^2}}{2\alpha n K_2^2(1/\Theta)} \left(1 + \frac{\sqrt{1+\bar{p}_z^2(\gamma, \xi)}}{\Theta} \right) \exp \left(-\frac{\gamma + \sqrt{1+\bar{p}_z^2(\gamma, \xi)}}{\Theta} \right) d\gamma, \quad (\text{C10})$$

513 which is Eq. 23.

514 Appendix D Derivation of non-relativistic $f_{\bar{p}_\perp}$

From Eq. A10,

$$f_{\bar{p}_\perp} = \frac{\bar{p}_\perp \sqrt{1+\bar{p}_\perp^2}}{\Theta K_2(1/\Theta)} K_1 \left(\frac{\sqrt{1+\bar{p}_\perp^2}}{\Theta} \right). \quad (\text{D1})$$

For $\bar{p}_\perp \ll 1$,

$$\sqrt{1+\bar{p}_\perp^2} \simeq 1 + \frac{\bar{p}_\perp^2}{2} \quad (\text{D2})$$

For $\Theta \ll 1$, it is seen that (Watson, 1995, Section 7.23)

$$K_2(1/\Theta) \simeq \sqrt{\frac{\pi\Theta}{2}} e^{-1/\Theta}, \quad (\text{D3})$$

and for small $\Theta \ll 1$ and $\bar{p}_\perp \ll 1$,

$$K_1\left(\frac{\sqrt{1+\bar{p}_\perp^2}}{\Theta}\right) \simeq K_1\left(\frac{1}{\Theta} + \frac{\bar{p}_\perp^2}{2\Theta}\right) \quad (\text{D4})$$

$$\simeq \sqrt{\frac{\pi\Theta}{2+\bar{p}_\perp^2}} \exp\left(-\frac{1}{\Theta} - \frac{\bar{p}_\perp^2}{2\Theta}\right), \quad (\text{D5})$$

so to lowest order,

$$f_{\bar{p}_\perp} \simeq \frac{\bar{p}_\perp}{\Theta} \sqrt{1 + \frac{\bar{p}_\perp^2}{2}} \exp\left(-\frac{\bar{p}_\perp^2}{2\Theta}\right) \quad (\text{D6})$$

$$\simeq \frac{\bar{p}_\perp}{\Theta} \exp\left(-\frac{\bar{p}_\perp^2}{2\Theta}\right). \quad (\text{D7})$$

The most likely \bar{p}_\perp value given this probability distribution function is

$$\bar{p}_{\perp, \text{ML}} = \sqrt{\Theta}. \quad (\text{D8})$$

515 Acknowledgments

516 The authors thank Mackenzie Wooten for reproducing some of the initial algebra. This
517 material is based upon work supported by the Air Force Office of Scientific Research un-
518 der award No. FA9550-17-1-0023 and by the NSF Division of Atmospheric and Geospace
519 Sciences under award No. 1914599. The associated scripts that generate data and plots
520 for this paper are available here: doi.org/10.22002/D1.1333

521 References

- 522 Akalin, F., Gurnett, D. A., Averkamp, T. F., Persoon, A. M., Santolik, O., Kurth,
523 W. S., & Hospodarsky, G. B. (2006, oct). First whistler observed in the
524 magnetosphere of Saturn. *Geophysical Research Letters*, *33*(20), L20107.
525 Retrieved from <http://doi.wiley.com/10.1029/2006GL027019> doi:
526 10.1029/2006GL027019
- 527 Albert, J. M. (2005). Evaluation of quasi-linear diffusion coefficients for whistler
528 mode waves in a plasma with arbitrary density ratio. *Journal of Geophysical*
529 *Research: Space Physics*, *110*(A3), 1–12. doi: 10.1029/2004JA010844
- 530 Anderson, K. A., & Milton, D. W. (1964, nov). Balloon observations of X rays in
531 the auroral zone: 3. High time resolution studies. *Journal of Geophysical Re-*
532 *search*, *69*(21), 4457–4479. Retrieved from [http://doi.wiley.com/10.1029/](http://doi.wiley.com/10.1029/JZ069i021p04457)
533 [JZ069i021p04457](http://doi.wiley.com/10.1029/JZ069i021p04457) doi: 10.1029/JZ069i021p04457
- 534 Artemyev, A., Agapitov, O., Mourenas, D., Krasnoselskikh, V., Shastun, V., &
535 Mozer, F. (2016). Oblique Whistler-Mode Waves in the Earth's Inner Mag-
536 netosphere: Energy Distribution, Origins, and Role in Radiation Belt Dy-
537 namics. *Space Science Reviews*, *200*(1-4), 261–355. Retrieved from [http://](http://dx.doi.org/10.1007/s11214-016-0252-5)
538 dx.doi.org/10.1007/s11214-016-0252-5 doi: 10.1007/s11214-016-0252-5
- 539 Artemyev, A. V., Vasiliev, A. A., Mourenas, D., Agapitov, O. V., & Krasnosel-
540 skikh, V. V. (2013, dec). Nonlinear electron acceleration by oblique whistler
541 waves: Landau resonance vs. cyclotron resonance. *Physics of Plasmas*, *20*(12),
542 122901. Retrieved from <http://aip.scitation.org/doi/10.1063/1.4836595>
543 doi: 10.1063/1.4836595
- 544 Barbosa, D. D., & Kurth, W. S. (1993). On the generation of plasma waves in
545 Saturn's inner magnetosphere. *Journal of Geophysical Research*, *98*(A6), 9351.
546 Retrieved from <http://doi.wiley.com/10.1029/93JA00477> doi: 10.1029/
547 93JA00477

- 548 Bellan, P. M. (2013, apr). Pitch angle scattering of an energetic magnetized parti-
 549 cle by a circularly polarized electromagnetic wave. *Physics of Plasmas*, *20*(4),
 550 042117. Retrieved from <http://aip.scitation.org/doi/10.1063/1.4801055>
 551 doi: 10.1063/1.4801055
- 552 Bellan, P. M. (2014, oct). Fast, purely growing collisionless reconnection as an
 553 eigenfunction problem related to but not involving linear whistler waves.
 554 *Physics of Plasmas*, *21*(10), 102108. Retrieved from [http://dx.doi.org/](http://dx.doi.org/10.1063/1.4897375)
 555 [10.1063/1.4897375](http://aip.scitation.org/doi/10.1063/1.4897375)
 556 doi: 10.1063/1.4897375
- 557 Bortnik, J., Thorne, R. M., & Inan, U. S. (2008, nov). Nonlinear interaction of
 558 energetic electrons with large amplitude chorus. *Geophysical Research Let-*
 559 *ters*, *35*(21), L21102. Retrieved from [http://doi.wiley.com/10.1029/](http://doi.wiley.com/10.1029/2008GL035500)
 560 [2008GL035500](http://doi.wiley.com/10.1029/2008GL035500) doi: 10.1029/2008GL035500
- 561 Boswell, R. W. (1984, oct). Very efficient plasma generation by whistler waves
 562 near the lower hybrid frequency. *Plasma Physics and Controlled Fusion*,
 563 *26*(10), 1147–1162. Retrieved from [http://stacks.iop.org/0741-3335/](http://stacks.iop.org/0741-3335/26/i=10/a=001?key=crossref.eb755a5ee079398ecf1bb3ffef2fb910)
 564 [26/i=10/a=001?key=crossref.eb755a5ee079398ecf1bb3ffef2fb910](http://stacks.iop.org/0741-3335/26/i=10/a=001?key=crossref.eb755a5ee079398ecf1bb3ffef2fb910) doi:
 565 10.1088/0741-3335/26/10/001
- 566 Bourdier, A., & Gond, S. (2000). Dynamics of a charged particle in a circularly po-
 567 larized traveling electromagnetic wave. *Physical Review E - Statistical Physics,*
 568 *Plasmas, Fluids, and Related Interdisciplinary Topics*, *62*(3 B), 4189–4206.
 569 doi: 10.1103/PhysRevE.62.4189
- 570 Breneman, A. W., Crew, A., Sample, J., Klumpar, D., Johnson, A., Agapitov,
 571 O., ... Kletzing, C. A. (2017). Observations Directly Linking Relativistic
 572 Electron Microbursts to Whistler Mode Chorus: Van Allen Probes and
 573 FIREBIRD II. *Geophysical Research Letters*, *44*(22), 11,265–11,272. doi:
 574 10.1002/2017GL075001
- 575 Burtis, W. J., & Helliwell, R. A. (1969, jun). Banded chorus-A new type of VLF
 576 radiation observed in the magnetosphere by OGO 1 and OGO 3. *Jour-*
 577 *nal of Geophysical Research*, *74*(11), 3002–3010. Retrieved from [http://](http://doi.wiley.com/10.1029/JA074i011p03002)
 578 doi.wiley.com/10.1029/JA074i011p03002 doi: 10.1029/JA074i011p03002
- 579 Cattell, C., Wygant, J. R., Goetz, K., Kersten, K., Kellogg, P. J., von Rosenvinge,
 580 T., ... Russell, C. T. (2008). Discovery of very large amplitude whistler-mode
 581 waves in earth's radiation belts. *Geophysical Research Letters*, *35*(1), 1–7. doi:
 582 10.1029/2007GL032009
- 583 Chai, K.-B., Zhai, X., & Bellan, P. M. (2016, mar). Extreme ultra-violet burst,
 584 particle heating, and whistler wave emission in fast magnetic reconnection in-
 585 duced by kink-driven Rayleigh-Taylor instability. *Physics of Plasmas*, *23*(3),
 586 032122. Retrieved from <http://dx.doi.org/10.1063/1.4944390>
 587 <http://aip.scitation.org/doi/10.1063/1.4944390> doi: 10.1063/1.4944390
- 588 Chen, F., & Boswell, R. (1997). Helicons-the past decade. *IEEE Transactions on*
 589 *Plasma Science*, *25*(6), 1245–1257. Retrieved from [http://ieeexplore.ieee](http://ieeexplore.ieee.org/document/650899/)
 590 [.org/document/650899/](http://ieeexplore.ieee.org/document/650899/) doi: 10.1109/27.650899
- 591 Coroniti, F. V., Kennel, C. F., Scarf, F. L., & Smith, E. J. (1982). Whistler
 592 mode turbulence in the disturbed solar wind. *Journal of Geophysical Re-*
 593 *search*, *87*(A8), 6029. Retrieved from [http://doi.wiley.com/10.1029/](http://doi.wiley.com/10.1029/JA087iA08p06029)
 594 [JA087iA08p06029](http://doi.wiley.com/10.1029/JA087iA08p06029) doi: 10.1029/JA087iA08p06029
- 595 Gao, X., Li, W., Thorne, R. M., Bortnik, J., Angelopoulos, V., Lu, Q., ... Wang,
 596 S. (2014, nov). Statistical results describing the bandwidth and coherence
 597 coefficient of whistler mode waves using THEMIS waveform data. *Journal of*
 598 *Geophysical Research: Space Physics*, *119*(11), 8992–9003. Retrieved from
 599 <http://doi.wiley.com/10.1002/2014JA020158>
 600 <http://doi.wiley.com/10.1002/2014JA020158> doi: 10.1002/2014JA020158
- 601 Ginet, G. P., & Heinemann, M. A. (1990, apr). Test particle acceleration by small
 602 amplitude electromagnetic waves in a uniform magnetic field. *Physics of Flu-*

- 603 *ids B: Plasma Physics*, 2(4), 700–714. Retrieved from [http://aip.scitation](http://aip.scitation.org/doi/10.1063/1.859307)
 604 [.org/doi/10.1063/1.859307](http://aip.scitation.org/doi/10.1063/1.859307) doi: 10.1063/1.859307
- 605 Greenberg, O. W. (2002, nov). $\langle \text{mi} \rangle C \langle \text{mi} \rangle$
 606 $\langle \text{mi} \rangle P \langle \text{mi} \rangle \langle \text{mi} \rangle T \langle \text{mi} \rangle$ Violation Implies Violation of
 607 Lorentz Invariance. *Physical Review Letters*, 89(23), 231602. Retrieved
 608 from <https://link.aps.org/doi/10.1103/PhysRevLett.89.231602> doi:
 609 10.1103/PhysRevLett.89.231602
- 610 Gurnett, D. A., & O'Brien, B. J. (1964, jan). High-latitude geophysical studies with
 611 satellite Injun 3: 5. Very-low-frequency electromagnetic radiation. *Journal of*
 612 *Geophysical Research*, 69(1), 65–89. Retrieved from [http://doi.wiley.com/](http://doi.wiley.com/10.1029/JZ069i001p00065)
 613 [10.1029/JZ069i001p00065](http://doi.wiley.com/10.1029/JZ069i001p00065) doi: 10.1029/JZ069i001p00065
- 614 Hairer, E., & Wanner, G. (1991). *Solving Ordinary Differential Equations II*
 615 (Vol. 14) (No. January 1996). Berlin, Heidelberg: Springer Berlin Heidel-
 616 berg. Retrieved from [http://link.springer.com/10.1007/978-3-319-32452-](http://link.springer.com/10.1007/978-3-319-32452-4)
 617 [4](http://link.springer.com/10.1007/978-3-319-32452-4) <http://link.springer.com/10.1007/978-3-662-09947-6> doi:
 618 10.1007/978-3-662-09947-6
- 619 Haw, M. A., Seo, B., & Bellan, P. M. (2019, jul). Laboratory Measurement of
 620 Large Amplitude Whistler Pulses Generated by Fast Magnetic Reconnec-
 621 tion. *Geophysical Research Letters*, 46(13), 7105–7112. Retrieved from
 622 <https://onlinelibrary.wiley.com/doi/abs/10.1029/2019GL082621> doi:
 623 10.1029/2019GL082621
- 624 Helliwell, R. A., & Crystal, T. L. (1973, nov). A feedback model of cyclotron
 625 interaction between whistler-mode waves and energetic electrons in the
 626 magnetosphere. *Journal of Geophysical Research*, 78(31), 7357–7371. Re-
 627 trieved from <http://doi.wiley.com/10.1029/JA078i031p07357> doi:
 628 10.1029/JA078i031p07357
- 629 Horne, R. B., & Thorne, R. M. (2003, may). Relativistic electron acceleration and
 630 precipitation during resonant interactions with whistler-mode chorus. *Geo-*
 631 *physical Research Letters*, 30(10). Retrieved from [http://doi.wiley.com/](http://doi.wiley.com/10.1029/2003GL016973)
 632 [10.1029/2003GL016973](http://doi.wiley.com/10.1029/2003GL016973) doi: 10.1029/2003GL016973
- 633 Hospodarsky, G. B., Averkamp, T. F., Kurth, W. S., Gurnett, D. A., Menietti,
 634 J. D., Santolik, O., & Dougherty, M. K. (2008, dec). Observations of
 635 chorus at Saturn using the Cassini Radio and Plasma Wave Science in-
 636 strument. *Journal of Geophysical Research: Space Physics*, 113(A12).
 637 Retrieved from <http://doi.wiley.com/10.1029/2008JA013237> doi:
 638 10.1029/2008JA013237
- 639 Jüttner, F. (1911). Das Maxwellsche Gesetz der Geschwindigkeitsverteilung
 640 in der Relativtheorie. *Annalen der Physik*, 339(5), 856–882. Retrieved
 641 from <http://doi.wiley.com/10.1002/andp.19113390503> doi: 10.1002/
 642 andp.19113390503
- 643 Kennel, C. F., & Petschek, H. E. (1966, jan). Limit on stably trapped particle
 644 fluxes. *Journal of Geophysical Research*, 71(1), 1–28. Retrieved from [http://](http://doi.wiley.com/10.1029/JZ071i001p00001)
 645 doi.wiley.com/10.1029/JZ071i001p00001 doi: 10.1029/JZ071i001p00001
- 646 Lakhina, G. S., Tsurutani, B. T., Verkhoglyadova, O. P., & Pickett, J. S. (2010,
 647 aug). Pitch angle transport of electrons due to cyclotron interactions with the
 648 coherent chorus subelements. *Journal of Geophysical Research: Space Physics*,
 649 115(A8). Retrieved from <http://doi.wiley.com/10.1029/2009JA014885>
 650 doi: 10.1029/2009JA014885
- 651 Leubner, M. P. (1982). On Jupiter's whistler emission. *Journal of Geophysi-*
 652 *cal Research*, 87(A8), 6335. Retrieved from [http://doi.wiley.com/10.1029/](http://doi.wiley.com/10.1029/JA087iA08p06335)
 653 [JA087iA08p06335](http://doi.wiley.com/10.1029/JA087iA08p06335) doi: 10.1029/JA087iA08p06335
- 654 Li, W., Thorne, R. M., Nishimura, Y., Bortnik, J., Angelopoulos, V., McFadden,
 655 J. P., ... Auster, U. (2010, jun). THEMIS analysis of observed equatorial elec-
 656 tron distributions responsible for the chorus excitation. *Journal of Geophysical*
 657 *Research: Space Physics*, 115(A6). Retrieved from <http://doi.wiley.com/>

- 658 10.1029/2009JA014845 doi: 10.1029/2009JA014845
- 659 Livadiotis, G. (2016, dec). Modeling anisotropic Maxwell-Jüttner distribu-
660 tions: derivation and properties. *Annales Geophysicae*, *34*(12), 1145–1158.
661 Retrieved from <https://www.ann-geophys.net/34/1145/2016/> doi:
662 10.5194/angeo-34-1145-2016
- 663 Lyons, L. R. (1974, dec). Pitch angle and energy diffusion coefficients from resonant
664 interactions with ioncyclotron and whistler waves. *Journal of Plasma Physics*,
665 *12*(3), 417–432. Retrieved from [https://www.cambridge.org/core/product/
666 identifier/S002237780002537X/type/journal-article](https://www.cambridge.org/core/product/identifier/S002237780002537X/type/journal-article) doi: 10.1017/
667 S002237780002537X
- 668 Lyons, L. R., Thorne, R. M., & Kennel, C. F. (1971, dec). Electron pitch-angle dif-
669 fusion driven by oblique whistler-mode turbulence. *Journal of Plasma Physics*,
670 *6*(3), 589–606. Retrieved from [https://www.cambridge.org/core/product/
671 identifier/S0022377800006310/type/journal-article](https://www.cambridge.org/core/product/identifier/S0022377800006310/type/journal-article) doi: 10.1017/
672 S0022377800006310
- 673 Macúšová, E., Santolík, O., Cornilleau-Wehrlin, N., & Yearby, K. H. (2015, feb).
674 Bandwidths and amplitudes of chorus-like banded emissions measured by
675 the TC-1 Double Star spacecraft. *Journal of Geophysical Research: Space
676 Physics*, *120*(2), 1057–1071. Retrieved from [http://doi.wiley.com/10.1002/
677 2014JA020440](http://doi.wiley.com/10.1002/2014JA020440) doi: 10.1002/2014JA020440
- 678 Mandt, M. E., Denton, R. E., & Drake, J. F. (1994, jan). Transition to whistler
679 mediated magnetic reconnection. *Geophysical Research Letters*, *21*(1), 73–76.
680 Retrieved from <http://doi.wiley.com/10.1029/93GL03382> doi: 10.1029/
681 93GL03382
- 682 Nunn, D. (1974, mar). A self-consistent theory of triggered VLF emis-
683 sions. *Planetary and Space Science*, *22*(3), 349–378. Retrieved from
684 <https://linkinghub.elsevier.com/retrieve/pii/0032063374900701>
685 doi: 10.1016/0032-0633(74)90070-1
- 686 Omura, Y., Furuya, N., & Summers, D. (2007, jun). Relativistic turning accel-
687 eration of resonant electrons by coherent whistler mode waves in a dipole
688 magnetic field. *Journal of Geophysical Research: Space Physics*, *112*(A6).
689 Retrieved from <http://doi.wiley.com/10.1029/2006JA012243> doi:
690 10.1029/2006JA012243
- 691 Omura, Y., Katoh, Y., & Summers, D. (2008, apr). Theory and simulation of
692 the generation of whistler-mode chorus. *Journal of Geophysical Research:
693 Space Physics*, *113*(A4). Retrieved from [http://doi.wiley.com/10.1029/
694 2007JA012622](http://doi.wiley.com/10.1029/2007JA012622) doi: 10.1029/2007JA012622
- 695 Omura, Y., Nunn, D., Matsumoto, H., & Rycroft, M. (1991, may). A review of
696 observational, theoretical and numerical studies of VLF triggered emissions.
697 *Journal of Atmospheric and Terrestrial Physics*, *53*(5), 351–368. Retrieved
698 from <https://linkinghub.elsevier.com/retrieve/pii/0021916991900312>
699 doi: 10.1016/0021-9169(91)90031-2
- 700 Omura, Y., & Summers, D. (2006, sep). Dynamics of high-energy electrons inter-
701 acting with whistler mode chorus emissions in the magnetosphere. *Journal of
702 Geophysical Research*, *111*(A9), A09222. Retrieved from [http://doi.wiley
703 .com/10.1029/2006JA011600](http://doi.wiley.com/10.1029/2006JA011600) doi: 10.1029/2006JA011600
- 704 Pierrard, V., & Lazar, M. (2010, nov). Kappa Distributions: Theory and Ap-
705 plications in Space Plasmas. *Solar Physics*, *267*(1), 153–174. Retrieved
706 from <http://link.springer.com/10.1007/s11207-010-9640-2> doi:
707 10.1007/s11207-010-9640-2
- 708 Qian, B.-L. (2000, feb). Relativistic motion of a charged particle in a super-
709 position of circularly polarized plane electromagnetic waves and a uni-
710 form magnetic field. *Physics of Plasmas*, *7*(2), 537–543. Retrieved from
711 <http://aip.scitation.org/doi/10.1063/1.873839> doi: 10.1063/1.873839
- 712 Roberts, C. S., & Buchsbaum, S. J. (1964, jul). Motion of a Charged Parti-

- 713 cle in a Constant Magnetic Field and a Transverse Electromagnetic Wave
 714 Propagating along the Field. *Physical Review*, 135(2A), A381–A389. Re-
 715 trieved from <https://link.aps.org/doi/10.1103/PhysRev.135.A381> doi:
 716 10.1103/PhysRev.135.A381
- 717 Russell, C. T., Holzer, R. E., & Smith, E. J. (1969, feb). OGO 3 observa-
 718 tions of ELF noise in the magnetosphere: 1. Spatial extent and frequency
 719 of occurrence. *Journal of Geophysical Research*, 74(3), 755–777. Re-
 720 trieved from <http://doi.wiley.com/10.1029/JA074i003p00755> doi:
 721 10.1029/JA074i003p00755
- 722 Santolík, O., Gurnett, D. A., Pickett, J. S., Chum, J., & Cornilleau-Wehrlin, N.
 723 (2009, dec). Oblique propagation of whistler mode waves in the chorus
 724 source region. *Journal of Geophysical Research: Space Physics*, 114(A12).
 725 Retrieved from <http://doi.wiley.com/10.1029/2009JA014586> doi:
 726 10.1029/2009JA014586
- 727 Sentman, D. D., & Goertz, C. K. (1978, jul). Whistler mode noise in Jupiter's
 728 inner magnetosphere. *Journal of Geophysical Research: Space Physics*,
 729 83(A7), 3151–3165. Retrieved from <http://doi.wiley.com/10.1029/JA083iA07p03151> doi: 10.1029/JA083iA07p03151
- 730 Sudan, R. N., & Ott, E. (1971, jul). Theory of triggered VLF emissions. *Journal of*
 731 *Geophysical Research*, 76(19), 4463–4476. Retrieved from [http://doi.wiley](http://doi.wiley.com/10.1029/JA076i019p04463)
 732 [.com/10.1029/JA076i019p04463](http://doi.wiley.com/10.1029/JA076i019p04463) doi: 10.1029/JA076i019p04463
- 733 Summers, D., Thorne, R. M., & Xiao, F. (1998). Relativistic theory of wave-
 734 particle resonant diffusion with application to electron acceleration in the
 735 magnetosphere. *Journal of Geophysical Research: Space Physics*, 103(A9),
 736 20487–20500. doi: 10.1029/98ja01740
- 737 Treumann, R. A., & Baumjohann, W. (2016, sep). Anisotropic Jüttner (relativis-
 738 tic Boltzmann) distribution. *Annales Geophysicae*, 34(9), 737–738. Retrieved
 739 from <https://www.ann-geophys.net/34/737/2016/> doi: 10.5194/angeo-34-
 740 -737-2016
- 741 Tsurutani, B. T., Lakhina, G. S., & Verkhoglyadova, O. P. (2013, may). En-
 742 ergetic electron (>10 keV) microburst precipitation, ~5-15 s X-ray pulsa-
 743 tions, chorus, and wave-particle interactions: A review. *Journal of Geo-*
 744 *physical Research: Space Physics*, 118(5), 2296–2312. Retrieved from
 745 <http://doi.wiley.com/10.1002/jgra.50264> doi: 10.1002/jgra.50264
- 746 Tsurutani, B. T., & Smith, E. J. (1974). Postmidnight chorus: A substorm phe-
 747 nomenon. *Journal of Geophysical Research*, 79(1), 118–127. doi: 10.1029/
 748 ja079i001p00118
- 749 Tsurutani, B. T., Southwood, D. J., Smith, E. J., & Balogh, A. (1993). A Survey of
 750 Low Frequency Waves at Jupiter: The Ulysses Encounter. *Journal of Geophys-*
 751 *ical Research*, 98(A12), 21203–21216. Retrieved from [http://doi.wiley.com/](http://doi.wiley.com/10.1029/93JA02586)
 752 [10.1029/93JA02586](http://doi.wiley.com/10.1029/93JA02586) doi: 10.1029/93JA02586
- 753 Tsurutani, B. T., Verkhoglyadova, O. P., Lakhina, G. S., & Yagitani, S. (2009,
 754 mar). Properties of dayside outer zone chorus during HILDCAA events:
 755 Loss of energetic electrons. *Journal of Geophysical Research: Space Physics*,
 756 114(A3). Retrieved from <http://doi.wiley.com/10.1029/2008JA013353>
 757 doi: 10.1029/2008JA013353
- 758 Vocks, C., Salem, C., Lin, R. P., & Mann, G. (2005, jul). Electron Halo and
 759 Strahl Formation in the Solar Wind by Resonant Interaction with Whistler
 760 Waves. *The Astrophysical Journal*, 627(1), 540–549. Retrieved from
 761 <http://stacks.iop.org/0004-637X/627/i=1/a=540> doi: 10.1086/430119
- 762 Watson, G. N. (1995). *A Treatise on the Theory of Bessel Functions*. Cambridge
 763 University Press.
- 764 Yoon, Y. D., & Bellan, P. M. (2017, may). A generalized two-fluid picture of non-
 765 driven collisionless reconnection and its relation to whistler waves. *Physics of*
 766 *Plasmas*, 24(5), 052114. Retrieved from <http://aip.scitation.org/doi/10>

768 .1063/1.4982812 doi: 10.1063/1.4982812
769 Yoon, Y. D., & Bellan, P. M. (2018, may). An intuitive two-fluid picture of spon-
770 taneous 2D collisionless magnetic reconnection and whistler wave generation.
771 *Physics of Plasmas*, 25(5), 055704. Retrieved from [http://dx.doi.org/](http://dx.doi.org/10.1063/1.5016345)
772 [10.1063/1.5016345](http://dx.doi.org/10.1063/1.5016345)
773 doi: 10.1063/1.5016345
774 Zwillinger, D. (2015). *Table of Integrals, Series, and Products*. Elsevier. Retrieved
775 from <https://linkinghub.elsevier.com/retrieve/pii/C20100648395> doi:
776 [10.1016/C2010-0-64839-5](https://doi.org/10.1016/C2010-0-64839-5)

Accepted Article